Biocompatibility and color stability of 3D printing resin containing TPO-L photoinitiator

Gi-Tae Kim

Department of Applied Life Science

The Graduate School, Yonsei University

Biocompatibility and color stability of 3D printing resin containing TPO-L photoinitiator

Directed by Professor Jae-Sung Kwon

The Master's Dissertation
submitted to the Department of Applied Life Science,
the Graduate School of Yonsei University
in partial fulfillment of the requirements for the degree of
Master in Applied Life Science

Gi-Tae Kim

June 2021

This certifies that the Master's Thesis of 'Gi-Tae Kim' is approved.

Thesis Supervisor: Jae-Sung Kwon

Thesis Committee Member#1: Kwang-Mahn Kim

Thesis Committee Member#2: Song-Yi Yang

The Graduate School
Yonsei University
June 2021

TABLE OF CONTENTS

LIST OF FIGURES

LIST OF TABLE

ABSTRACT

Biocompatibility and color stability of 3D printing resin containing TPO-L photoinitiator

Gi-Tae Kim

Department of Applied Life Science

The Graduate School, Yonsei University

(Directed by Professor Jae-Sung Kwon, M.D., Ph.D.).

Objectives

Three-dimensional printing system has been a significant impact on the dental polymer-based restorative material by simplifying the manufacturing process and reducing manufacturing time. The resin material used for DLP 3D printing is a light-cured resin. BAPO and TPO photoinitiators have been used as photoinitiators for 3D printed resins due to the advantages of high polymerization efficiency and an excellent rate of polymerization. However, there were problems with cytotoxicity and discoloration. On the other hand, TPO-L photoinitiator has good biocompatibility and excellent color stability. Few studies have used TPO-L photoinitiator as a DLP 3D Printing

photoinitiator. Therefore, the purpose of this study is to evaluate the cytotoxicity, color stability, dimensional accuracy, degree of conversion, mechanical and physical properties for 3D printed resins using TPO-L as the photoinitiator to evaluate their potential for utilization as a dental 3D printing photoinitiator.

Materials and methods

70 wt% UDMA, 20 wt% Bis-EMA and 10 wt% TEGDMA were used as 3D printing resin matrix. BAPO, TPO and TPO-L were used as photoinitiators and 0.1 mol% of each photoinitiator was mixed with the resin matrix to prepare a 3D printing resin mixture. The specimens were designed using a CAD program and printed by a DLP 3D printer. The 3D-printed specimens were washed with IPA for 5 min, polymerized in a post-curing unit for 15 min. The experiments measured cytotoxicity, color stability, dimensional accuracy, degree of conversion, mechanical and physical properties.

Results

In the cytotoxicity test of 3D printed resin groups, the TPO-L group showed significantly higher cell viability than the BAPO and TPO groups ($p < 0.05$). In cytotoxicity test with photoinitiators by concentration, TPO-L photoinitiator represented high cell viability at all concentrations, while BAPO and TPO showed significantly low cell viability at 25 μM and 50 μM concentrations ($p < 0.05$). In the color stability test, the TPO-L group revealed the highest color stability and showed no significant difference from the TPO group ($p > 0.05$). However, the BAPO group revealed the lowest color stability and showed significant differences from other groups ($p < 0.05$). Accuracy of the Z-axis revealed that the TPO-L group was closest to the true value. Z-axis value of TPO group was secondly similar to the true value. The accuracy of the XY-axis revealed that the TPO group was closest to the true value. XY-axis value of

TPO-L group was secondly similar to the true value. The BAPO group showed significantly lower accuracy on the Z-axis and XY-axis ($p<0.05$). The degree of conversion and mechanical properties were not significantly different for all groups ($p>0.05$). The physical properties, water sorption and solubility, showed significantly lower results for the BAPO group ($p<0.05$).

Significance

In this study, TPO-L photoinitiator showed excellent biocompatibility, color stability and revealed acceptable dimensional accuracy for use in 3D printing resins. Therefore, the TPO-L photoinitiator can solve the problems of BAPO and TPO photoinitiators and can be sufficiently used as a photoinitiator for dental 3D printing resin.

Key words: 3D printing accuracy, Color stability, Cytotoxicity, DLP 3D printing, TPO-L photoinitiator

Biocompatibility and color stability of 3D printing resin containing TPO-L photoinitiator

Gi-Tae Kim

Department of Applied Life Science
The Graduate School, Yonsei University

(Directed by Professor Jae-Sung Kwon, M.D., Ph.D.)

I. INTRODUCTION

1. Additive manufacturing and dental 3D printer

Traditional dental prostheses have been manufactured in multiple stages. The Computer-Aided Design/Computer-Aided Manufacturing (CAD/CAM) system has been a major impact on the dental field by simplifying the process and reducing production time (Abduo et al., 2014; Van Noort, 2012). The CAM system is divided into additive manufacturing and subtractive manufacturing. 3D printing system that corresponds to additive manufacturing has the advantage of being able to create complex shapes, personalized production and consuming less material (Della Bona et al., 2021; Moon et al., 2021). The 3D printing system is a method of printing standard tessellation language (STL) files with a 3D printer. Most of 3D printers used in dentistry are polymer-based printers. Dental 3D printing resins can be used to make prostheses such as surgical guides, crowns & bridges, and dentures (Stansbury and Idacavage, 2016).

Among the 3D printing methods, Digital Light Processing (DLP) is the promising 3D printing technology in dental applications because of its rapid processing, low cost and high resolution (Revilla-León and Özcan, 2019). The DLP technology is the method of irradiating light in tanks containing light-cured resin which reacts with ultraviolet and producing prosthetics through photo-polymerization (Moon et al., 2021).

1

2. Degree of conversion of light-cured resin

Light-cured resin is used for various purposes and it is mainly used as a direct and indirect restorative material for anterior and posterior teeth. Ingredients of light-cured resin are composed of a matrix that is considered the "active component" and fillers to ensure the properties of the material (Albuquerque et al., 2013).

The matrix of resin prosthesis is mostly composed of dimethacrylate monomers such as Bis-GMA (bisphenol-glycidyl dimethacrylate), UDMA (urethane dimethacrylate), Bis-EMA (Bisphenol A ethoxylate dimethacrylate) or TEGDMA (triethyleneglycol dimethacrylate). In addition, a photoinitiator system is added to the resin matrix in order to trigger the process of free radicals to complete the polymerization reaction (Peutzfeldt, 1997). The degree of conversion of methacrylate-based materials has a significant impact on the biological, physical and mechanical properties of the polymer and ultimately determines the life of the restoration (Stansbury, 2012; Van Landuyt et al., 2011). The degree of conversion of dimethacrylate-based dental resins can range from 50 % to over 80 %, mainly depending on the material and curing conditions (Gonçalves et al., 2009). The degree of conversion is affected by several factors, such as the type of methacrylate monomer, temperature, light intensity, and the kind and concentration of the photoinitiator system (Andrzejewska, 2001; Ikemura and Endo, 2010). Since efficient radical polymerization initiators are a greatly valuable component of light-cured resin, a lot of research was conducted to develop the most effective photoinitiator systems (Meereis et al., 2014).

3. Photoinitiator

3.1. Types and reactions of photoinitiators

Photoinitiator system is required to trigger polymerization of the monomer by photoactivation. Photoinitiators are divided into Norrish type I photoinitiators and Norrish type II photo-initiators (Salgado et al., 2017).

Norrish Type I photoinitiator, the photoinitiator molecule is cleaved to generate radicals after light absorption.

Norrish Type II photoinitiator becomes an excited state after light absorption and receives the electron of the co-initiator to generate radicals.

3.2. Usable photoinitiators for 3D printing

A commonly used photoinitiator in dentistry is camphorquinone (CQ), which is a Norrish type II molecule. It uses a tertiary amine as the main co-initiator and has an absorption wavelength band of 450 ~ 500 nm (λmax = 468 nm) (Meereis et al., 2014). CQ has been used frequently in light-cured resin composite. But CQ is yellowish and the amines of the co-initiator undergo yellowing over time, which may impair aesthetics (Neumann et al., 2006). Furthermore, the polymerization reaction is slower than that of the Norrish type I molecules, and it is difficult to polymerize at a UV wavelength, which is a light source used in a 3D printer. Due to these limitations, the photoinitiators used in 3D printing systems are primarily Norrish type I (Lai et al., 2019).

Among the Norrish type I, the phosphine oxide series, unlike CQ, do not require a co-initiator and has the advantages of the excellent degree of conversion, rate of polymerization and color stability (Popal et al., 2018).

Representative Norrish type I photoinitiators are phenylbis phosphine oxide and diphenyl phosphine oxide.

3.2.1. Problems of phenylbis phosphine oxide and diphenyl phosphine oxide

Phenylbis (2,4,6-trimethylbenzoyl) phosphine oxide (BAPO) has been often used as a photoinitiator in 3D printing resins (Lai et al., 2019). BAPO has a high light absorptivity and can divide up to 4 radicals per molecule, so the polymerization efficiency is excellent (Almeida et al., 2020). However, it is known to be highly cytotoxic and cause discoloration (Zeng et al., 2021).
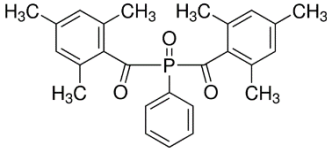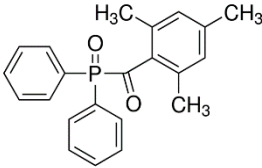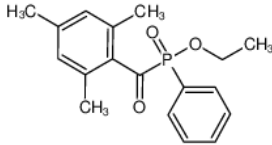
Diphenyl (2,4,6-trimethylbenzoyl) phosphine oxide (TPO) has been extensively studied as a photoinitiator for polymer-based composites (de Oliveira et al., 2016; Pongprueksa et al., 2014; Schneider et al., 2012). TPO be divide into two radicals, has a higher degree of conversion than CQ, and has better color stability than BAPO (Manojlovic et al., 2016). However, the higher cytotoxicity than CQ and lower polymerization efficiency than BAPO remained a problem (Almeida et al., 2020).

3.2.2. Advantages of ethyl phenylphosphinate

Ethyl (2,4,6-trimethylbenzoyl) phenylphosphinate (TPO-L) has rarely been studied as a dental photoinitiator. Zeng et al. reported that TPO-L showed the highest biocompatibility and excellent transparency among the seven photoinitiators (Zeng et al., 2021). And, Steyrer et al. evaluated that TPO-L represents a higher degree of conversion than BAPO (Steyrer et al., 2017). The advantages of TPO-L described above can solve the problems of BAPO and TPO photoinitiators.

Table 1 shown the chemical structure and molecular weight of the mentioned photoinitiators.

Table 1. Chemical structures of tested photoinitiators.

Photoinitiator	Structure	Molecular Weight
Phenylbis (2,4,6-trimethylbenzoyl) phosphine oxide (**BAPO**)		418.5
Diphenyl (2,4,6-trimethylbenzoyl) phosphine oxide (**TPO**)		348.4
Ethyl (2,4,6-trimethylbenzoyl) phenylphosphinate (**TPO-L)**		316.4

www.sigmaaldrich.com, www.molbase.com

4. Research objectives

The 3D printing resins are available with a wide range of photoinitiators, such as dental polymer-based restorations. The BAPO and TPO photoinitiators, which are mainly used for 3D printing, have the advantages of a high degree of conversion and rate of polymerization but have disadvantages such as cytotoxicity and discoloration.

Few studies have applied TPO-L to dental 3D printing resins to solve the problem of BAPO and TPO photoinitiators. Therefore, the purpose of this study is to evaluate that the TPO-L photoinitiator is sufficiently usable as a dental 3D printing photoinitiator.

The null hypothesis was that there would be no difference in cytotoxicity, color stability, 3D printing accuracy, degree of conversion, mechanical and physical properties between dental 3D printing resin with three different photoinitiators.

II. MATERIALS AND METHODS

1. Materials

In this study, Bisphenol-A-ethoxy dimethacrylate (Bis-EMA; Sigma-Aldrich, Steinheim, Germany), Urethane dimethacrylate (UDMA; Sigma-Aldrich, Steinheim, Germany), and Triethyleneglycol dimethacrylate (TEGDMA; Sigma-Aldrich, Steinheim, Germany) were used for the 3D printing resin matrix.

The photoinitiators used in the experiment were Phenylbis (2,4,6-trimethylbenzoyl) phosphine oxide (BAPO; IGM Resins, Waalkwijk, Netherlands), Diphenyl (2,4,6-trimethylbenzoyl) phosphine oxide (TPO; IGM Resins, Waalkwijk, Netherlands), and Ethyl (2,4,6-trimethylbenzoyl) phenylphosphinate (TPO-L; IGM Resins, Waalkwijk, Netherlands).

2. Characterization of the absorption spectra of each photoinitiator

Spectrophotometric analysis was performed to confirm that the absorption spectra of the photoinitiator were consistent with the emission wavelength band of the 3D printer and post-curing unit. Each initiator (0.0041 g of BAPO, 0.0034 g of TPO and 0.0031 g of TPO-L) was completely dissolved in 10 mL of toluene (Sigma-Aldrich, Steinheim, Germany). The concentration of the dissolved photoinitiator was 1 mM. These concentrations were selected to match the mole ratio of initiators in the materials as tested. The 2 mL of solution was placed in UV-transparent cuvettes and UV–vis spectra (350 ~ 500 nm) were obtained using a UV–vis spectrophotometer (V-650; JASCO, Hachioji, Japan), with 0.5 nm sampling interval and 200 nm/min scan speed.

3. Preparation of experimental 3D printing resin

3.1. Preparation of 3D printing resin matrix

Experimental 3D printing resin matrix was formulated in the ratio as in Table 2. The mixed resin matrix was divided into three groups according to three different photoinitiators. The resin mixture in a light-resistant container was added photoinitiator at 0.1 mol% and mixed using a magnetic stirrer device in a dark environment at 60 °C for 20 min.

As shown in Figure 1, the mixed 3D printing resins were grouped by the name of the photoinitiator added to each group.

Table 2. Composition of 3D Printing resin matrix.

Composition	Wt.%
Urethane dimethacrylate (UDMA)	70
Bisphenol A ethoxylate dimethacrylate (Bis-EMA)	20
Triethylene glycol dimethacrylate (TEGDMA)	10
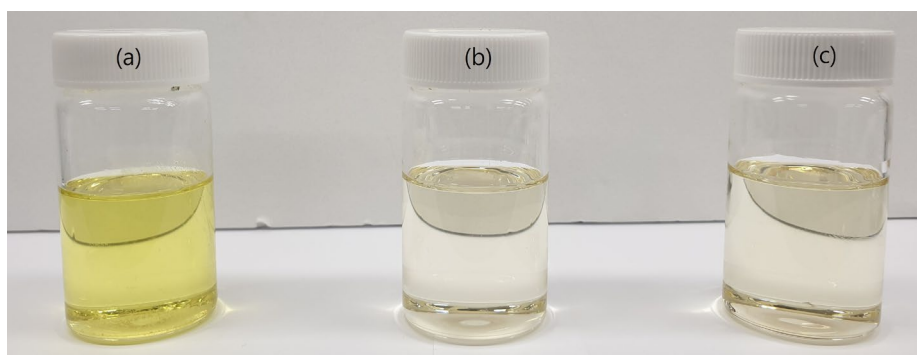
Figure 1. Mixed 3D printing resin. (a) BAPO group, (b) TPO group, (c) TPO-L group.

3.2. Preparation of 3D printed specimens

3D Sprint software (NextDent Co., Seosterberg, Netherlands) was used for designing the specimen. The Specimens required for each test were designed. The completed design was positioned in slicing software (VeltzBP; Veltz 3D Co., Incheon, Korea) and after adding a supporter to the specimen design, it was converted to a standard tessellation language format.

All specimens were manufactured using a DLP printer (D2; Veltz 3D Co., Incheon, Korea). The wavelength is 405 nm and the accuracy is $\pm$ 2 µm. The layer thickness was set to 100 µm, and the light exposure time of the specimen was set to 5.5 s. The 3D-printed green phase specimen was placed in a beaker containing isopropyl alcohol (IPA; LG Chem Ltd., Yeosu, Korea) and ultrasonically cleaned for 3 min. After that, the supporter was removed and ultrasonic cleaning was performed for 2 min in the same method. After that, support structures were removed using the finish kit (Form 2 Finish Kit; Formlabs Inc., Somerville, MA, USA) and ultrasonic cleaning was performed for 2 min in the same method. After removing all remaining IPA with an air gun, specimens were put into a post-curing unit (LC-3D Print Box; NextDent Co., Seosterberg, The Netherlands) with a wavelength band of 350 ~ 500 nm and cured for 15 min.

4. Cytotoxicity test

To evaluate the cytotoxic effects of each photoinitiator and 3D printed resin, a cytotoxicity test was carried out by using the 3-(4,5-dimethylthiazol-2-yl)-2,5-diphenyltetrazolium bromide (MTT) assay according to the ISO 10993-5:2009 standard (ISO, 2009).

4.1. Preparation of cell culture

The L-929 mouse fibroblasts were cultured in RPMI-1640 cell culture medium (Welgene, Gyeongsangbuk-do, Korea) containing 10 % fetal bovine serum (FBS; Gibco, Grand Island, NY, USA) and 1 % penicillin streptomycin (Gibco, Grand Island, NY, USA). The cell suspension was prepared at a concentration of 1×10^5 cell/ml and inoculated onto 96-well cell culture plates (100 µl/well). The multi-well plates were incubated at 37 °C, with 5 % CO_2 in air for 24 h.

4.2. Cytotoxicity evaluation of extracts or diluted solution according to experimental materials

4.2.1. Extracts of 3D printed resin containing each photoinitiator

The specimen of cytotoxicity test was disc-shaped, 10 mm in diameter and 5 mm in height. Specimen preparation was performed in the same method as in 3.2. The residual supporters of 3D printed specimen were polished to #1000 grit silicon carbide (SiC) paper.

Following the ISO standard 10993-12:2012 (ISO, 2012), the extract was prepared by soaking specimens in culture medium RPMI-1640 at a concentration of 3 cm²/mL. The extraction was carried out at 37 °C for 24 h.

The blank control group used RPMI-1640 eluted at 37 °C for 24 h. The positive control group used 1 % phenol (Sigma-Aldrich, Steinheim, Germany). The medium of the cultured L929 cells was then replaced by equal volumes (100 µl) of the extracts and incubated at 37 °C, 5% CO_2 in air for 24 h.

4.2.2. Diluted solution of photoinitiators

A stock solution of BAPO, TPO and TPO-L photoinitiators was dissolved to reach 100 μM in DMSO and freshly diluted in medium prior to each experiment (final DMSO concentration: 1 %). Final concentrations of photoinitiators used in MTT assays were between 1 μM and 50 μM. All solutions were prepared under dim room light and wrapped in aluminum foil to block the light.

The blank control group used RPMI-1640 eluted at 37 °C for 24 h. The negative control group used 1 % DMSO and positive control group used 1 % phenol. The medium of the cultured L929 cells was then removed and L929 cells cultured in a diluted solution of each photoinitiator at 1 μM, 5 μM, 10 μM, 25 μM and 50 μM concentrations at 37 °C, 5 % CO_2 in air for 24 h.

4.3. Methylthiazol tetrazolium (MTT) assay

Following removal of the test extracts, 50 µl MTT solution with a concentration of 1 mg/mL was added to each well and incubated in a dark environment for 2 h at 37 °C. MTT solution was removed and 100 µl isopropanol (Sigma-Aldrich, Steinheim, Germany) was added to each well. The IPA-treated plate was shaken with a rotator (C-SKS; Changshin Science, Seoul, Korea) for 30 minutes. The absorbance at 570 nm was measured using a microplate spectrophotometer (Epoch; Biotek, Winooski, USA). The cell viability was calculated using the following equations:

$$\text{Viab.}\% = \frac{100 \times OD_{570e}}{OD_{570b}}$$

Where, OD_{570e} is the value of the measured optical density of the extracts of the test sample, OD_{570b} is the value of the measured optical density of the blank.

5. Color stability

5.1. Design and printing for color stability test

The color stability after irradiation and water sorption of the 3D printing resin was performed according to ISO 4049:2019 (ISO, 2019). The specimen was disc-shaped, 15 mm in diameter and 1.0 mm in height. Specimen preparation was performed in the same method as in 3.2.
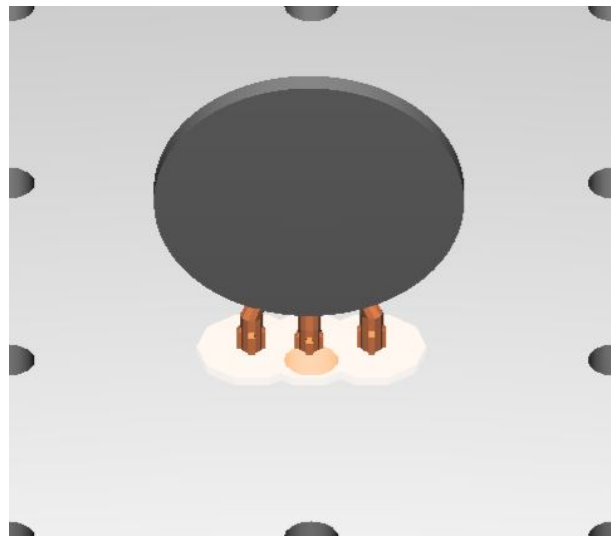
Figure 2. STL image of color stability specimen.

5.2. Color stability test

Specimens used in the color stability test were prepared based on Figure 3. The CIELAB coordinates of each specimen were measured using a spectrophotometer (CM-3500d; Konica Minolta, Sensing Inc., Japan). Three sites were measured at random for each specimen, and the mean value and standard deviation were obtained. The classified specimens were performed color comparison (ΔE) based on ISO 4049:2019 (ISO, 2019). ΔE was calculated using the equation:

$$\Delta E = [(\Delta L^*)^2 + (\Delta a^*)^2 + (\Delta b^*)^2]^{1/2}$$
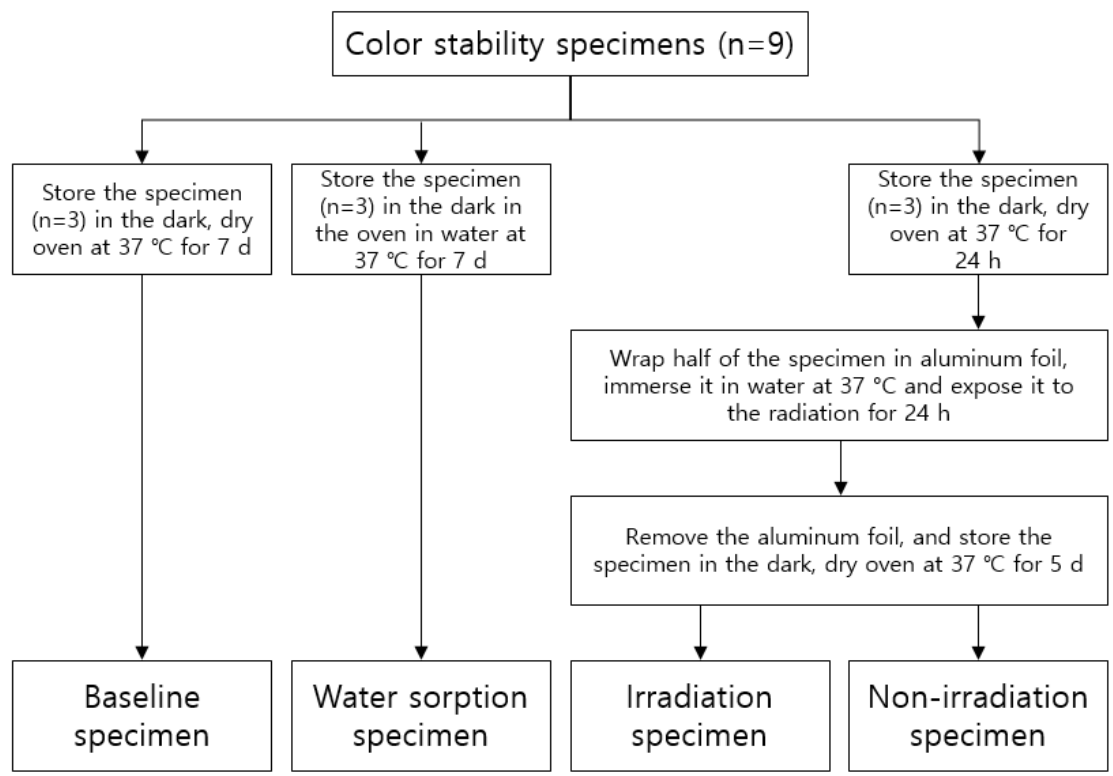
Figure 3. Classification of specimens for color stability test.

6. Dimensional accuracy of 3D printed specimens

6.1. Design and printing for dimensional accuracy test

The 3D printing accuracy specimen (n=3) was prepared in the shape of a die based on Figure 4. Specimen preparation was performed in the same method as in 3.2. The supporters were not removed and were mounted on the plate of the model scanner.
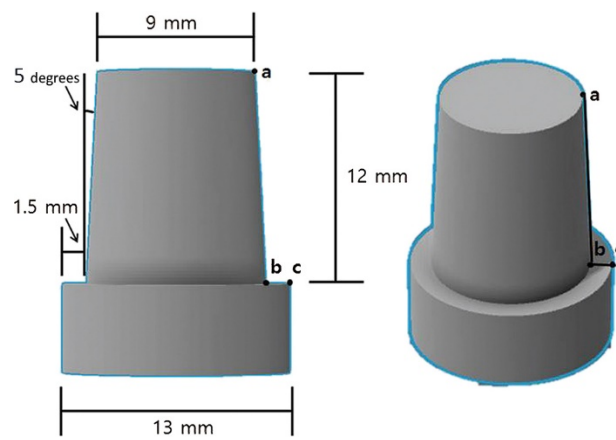
Figure 4. Specimen design for 3D printing accuracy test (Park and Shin, 2018).
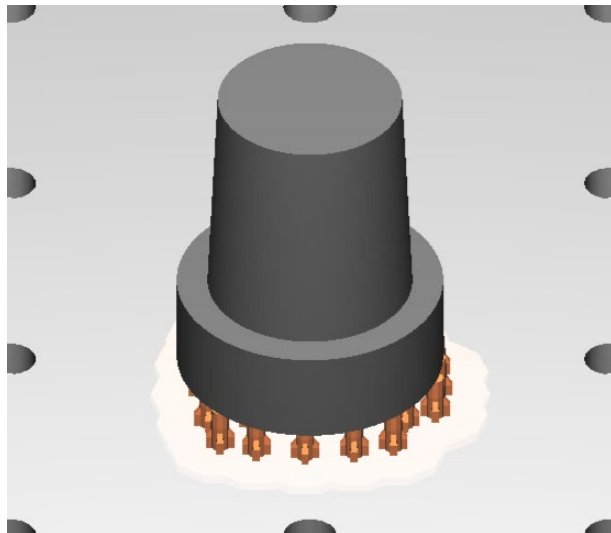
Figure 5. STL image of specimen for 3D printing accuracy test.

6.2. Evaluation for dimensional accuracy

The fabricated specimens were scanned with the light model scanner (Medit T710; Medit, Seoul, Korea) by groups after spraying scan powder (EASY SCAN SPRAY; Alphadent, Gyeonggi-do, Korea) on the surface of the specimens. Dimensional accuracy between the original STL data and three different groups was compared by the best-fit alignment using a 3D inspection software (Geomagic control X; 3D Systems, Rock Hill, SC, USA). After that, 2-dimensional (2D) analysis was performed by dividing the superimposed data equally in the vertical axial. The maximum and minimum range was set at ± 0.5 mm, and tolerance levels were set at ± 0.05 mm. Each specimen was measured three times as shown in figure 6, the average value was calculated, and used.
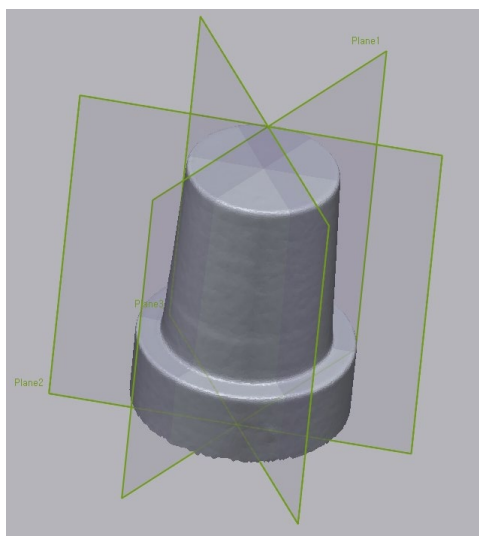
Figure 6. Plane division for 2D analysis.

7. Degree of conversion

7.1. Design and printing for degree of conversion test

The specimens (n=3) with a diameter of 10 mm and a height of 2 mm were prepared in accordance with same method as in 3.2. The prepared disk specimens were polished with #1200 grit silicon carbide (SiC) paper using a water-cooled rotating polishing machine (Ecomet 30; Buehler Ltd., Lake Bluff, IL, USA).
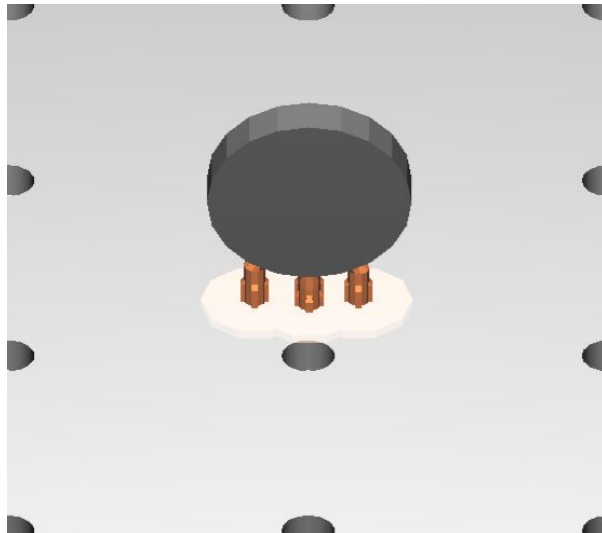
Figure 7. STL image of specimen for degree of conversion test

7.2. Degree of conversion analysis

Fourier-transform infrared spectroscopy (FT-IR) spectra were recorded using an FT-IR spectrometer (Nicolet iS10, Thermo Scientific, Waltham, MA, USA) with attenuated total reflection (ATR, diamond crystal) accessories. The spectra were obtained in the range of 4000 ~ 500 cm^{-1} with a total of 32 scans per spectrum and a resolution of 4 cm^{-1}. Three specimens from each experimental group were printed and processed post-curing. Each specimen was measured three times with FT-IR, the average value was calculated, and used.

All spectrums were referenced to the carbonyl group (C=O peak) at 1720 cm^{-1}, and the degree of conversion of each specimen was determined by comparing the intensity of the aliphatic C=C stretching vibration at 1638 cm^{-1} of the polymerized 3D printing resin and uncured 3D printing resin. The degree of conversion (DC) was determined according to the following equation:

$$DC\ (\%) = \left[1 - \frac{(1638cm^{-1}/1720cm^{-1})cured}{(1638cm^{-1}/1720cm^{-1})uncured}\right] \times 100$$

8. Mechanical properties

8.1. Three-point flexural strength

8.1.1. Design and printing for three-point flexural strength test

The specimen (n=15) of three-point flexural strength was referenced to the ISO 4049:2019 standard (ISO, 2019). The specimen for three-point flexural strength test was printed with size of 25 mm × 2 mm × 2 mm.

Specimen preparation was performed in the same method as in 3.2. The residual supporters of 3D printed specimen were polished using a water-cooled rotating polishing machine (Ecomet 30; Buehler Ltd., Lake Bluff, IL, USA) with #320 grit silicon carbide (SiC) paper.
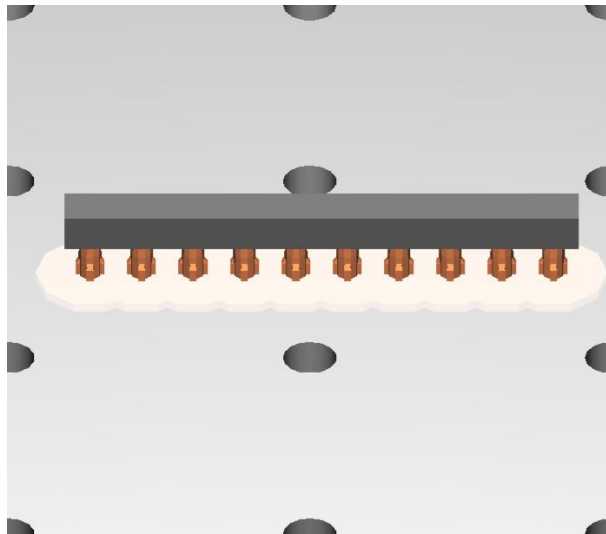
Figure 8. STL image of three-point flexural strength specimen.

8.1.2. Three-point flexural strength test

Three-point flexural strength test was carried out on a universal testing machine (Instron 5942; Instron, Norwood, MA, USA). The crosshead speed was 1 mm/min and the distance between the two rounded supports was 20 mm. The load was applied until the specimen was fractured. The maximum load was recorded and the flexural strength (S) was calculated using the following equation:

$$S = \frac{3FL}{2bh^2}$$

Where F is the maximum fracture load, L is the distance of support (20 mm), b is the width of specimen, and h is height of specimen.

8.2. Microhardness

8.2.1. Design and printing for microhardness test

The specimen (n=10) for microhardness test was disc-shaped, 10 mm in diameter and 5 mm in height. Specimen preparation was performed in the same method as in 3.2. The prepared disk specimens were polished with #400, #800 and #1200 grit silicon carbide (SiC) paper a using water-cooled rotating polishing machine (Ecomet 30; Buehler Ltd., Lake Bluff, IL, USA).
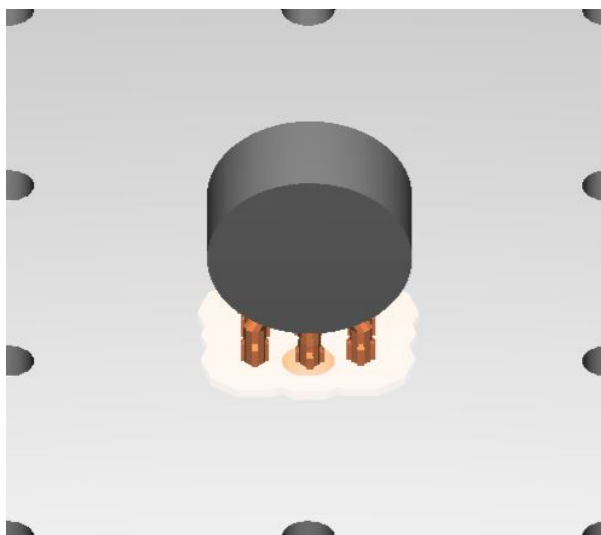
Figure 9. STL image of microhardness specimen.

8.2.2. Microhardness test

The samples were placed in a Knoop hardness tester (DMH-2; Matsuzawa Seiki Ltd., Tokyo, Japan), and 0.98 N (100 gf) was applied for 25 s. The indentation was observed, and the Knoop hardness number (KHN) was measured to determine the surface hardness. Three sites were measured at random for each specimen, and the mean value and standard deviation were obtained. The hardness was determined using the following equation:

$$\text{KHN} = 14.229 P d^2$$

Where P is the indentation load and d the long diagonal length of the Knoop indentation.

9. Physical properties

9.1. Water sorption and solubility

9.1.1. Design and printing for water sorption and solubility test

The water absorption and solubility of the 3D printing resin were performed according to ISO 4049:2019 (ISO, 2019). The specimen (n=10) of water sorption and solubility was disc-shaped, 15 mm in diameter and 1.0 mm in height. Specimen preparation was performed in the same method as in 3.2. The residual supporters of 3D printed specimen were polished to #1000 grit silicon carbide (SiC) paper.
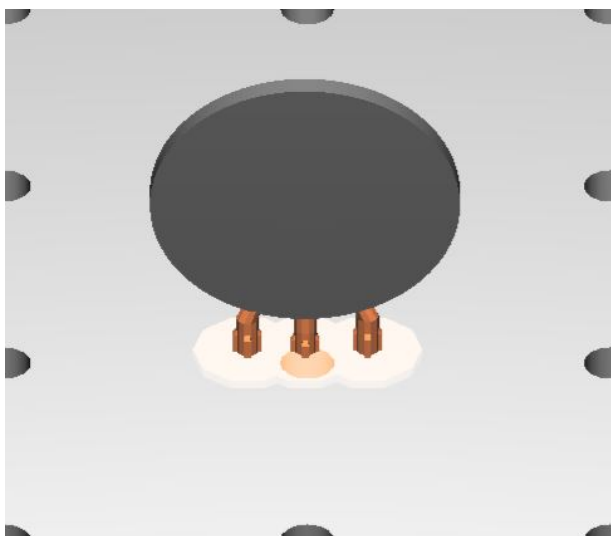
Figure 10. STL image of water sorption and solubility specimen.

9.1.2. Water sorption and solubility test

The specimen was placed in a desiccator maintained at (37 ± 2) ˚C. After 22 h, the specimens were removed and stored in a desiccator at (23 ± 1) ˚C for 2 h, and then they were weighed in an analytical balance accurate to 0.01 mg (XS105; Mettler-toledo AG, Greifensee, Switzerland) with a reproducibility of 0.1 mg until a constant mass (m_1) was obtained.

The diameter and thickness of the specimen were measured using a digital caliper accurate to 0.01 mm (Mitutoyo Model CD-15CPX; Mitutoyo Corporation, Kawasaki, Japan). The mean diameter value of specimen was calculated by measuring three diameters, and the mean thickness value of specimen was calculated by measuring three equally spaced points on the circumference. These values were then used to calculate the volume (V) of all samples (in 0.01 mm^3).

Following these procedures, they were stored for 7 d in distilled water at (37 ± 1) ˚C, blotted until free from visible moisture, waved in the air at 15 s, and weighed for mass (m_2).

Finally, each disk was placed in a desiccator and weighed daily until a constant dry mass (m_3) was obtained. Water sorption and solubility were calculated using the following equations:

$$W_{sp} = \frac{(m_2 - m_3)}{V}$$

$$W_{sl} = \frac{(m_1 - m_3)}{V}$$

Where W_{sp} is the absorption of the test material (μg/mm^3), W_{sl} is the solubility of the test material (μg/mm^3).

10. Statistical analysis

To evaluate the properties of the 3D printing resin according to photoinitiators, the results of cytotoxicity test, color stability (ΔE), degree of conversion, mechanical properties and physical properties data were analyzed with one-way ANOVA followed by Tukey's statistical test. The results of dimensional accuracy data were analyzed with Kruskal-Wallis test followed by Mann-Whitney post hoc test.

All statistical analyses were performed using the SPSS 25 software program (IBM, Armonk, NY, USA). The all statistical significance levels were set at a confidence 95 %.

III. RESULTS

1. Characterization of the absorption spectra of each photoinitiator

The absorption spectra were obtained from the UV-vis spectrophotometer; this is shown in Figure 11. The absorption wavelength band of BAPO showed 350 ~ 450 nm, and TPO and TPO-L showed the absorption wavelength band of approximately 350 ~ 430 nm. The emission wavelength band of 3D printer and post-curing unit was 350 ~ 500 nm. Therefore, it was confirmed that the three photoinitiators can sufficiently generate a radical reaction in the emission wavelength band of the 3D printer and the post-curing unit.
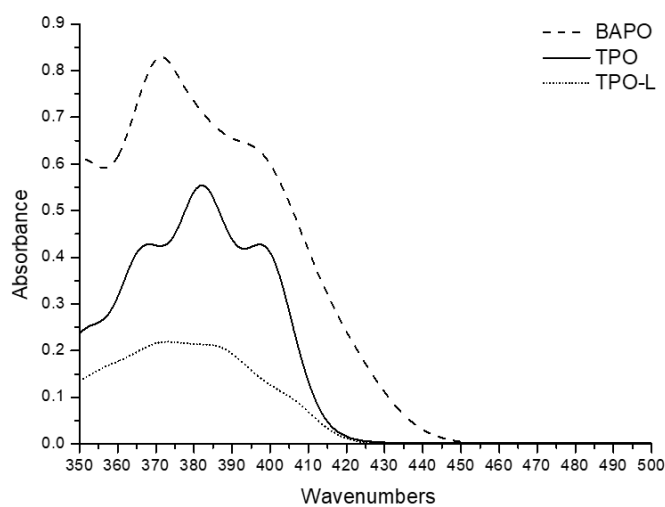
Figure 11. Absorption spectra for each photoinitiator (BAPO: phenylbis(2,4,6-trimethylbenzoyl) phosphine oxide, TPO: diphenyl (2,4,6-trimethylbenzoyl) phosphine oxide, and TPO-L: ethyl (2,4,6-trimethylbenzoyl) phenylphosphinate).

2. Cytotoxicity test

2.1. Cytotoxicity of 3D printed resin extracts containing each photoinitiator

The results of the cytotoxicity test of 3D printed resin are shown in Figure 12, which revealed significant differences among all the groups ($p<0.05$). TPO-L group had the highest cell viability of (89.62 ± 4.93) %, while BAPO group had the lowest cell viability of (74.16 ± 3.7) %. The cell viability of TPO group was (84.45 ± 3.62) %. The cell viability of positive control was (6.77 ± 1.66) %.
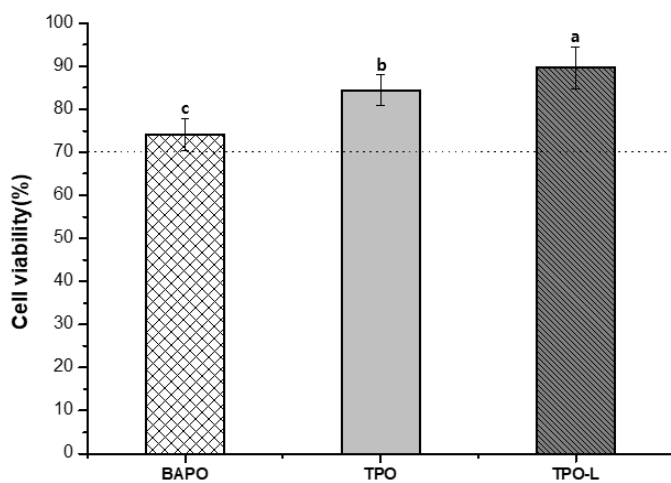
Figure 12. Cell viability of 3D printed resin groups. Each value represents the mean of 9 measurements, and the error bars represent the standard deviation of the mean (mean ± standard deviation). Differences in lowercase alphabetical letters above the bar graph indicate significant difference of each group ($p<0.05$).

2.2. Cytotoxicity of photoinitiators

The results of the cytotoxicity test of each photoinitiator are shown in Figure 13. The cell viability of positive control and negative control was (7.58 ± 1.6) % and (95.8 ± 5.3) %. BAPO photoinitiator showed the cell viability of (92.98 ± 6.93) % at 1 μM, (83.69 ± 9.69) % at 5 μM, (83.12 ± 10.11) % at 10 μM, (70.44 ± 11.84) % at 25 μM and (56.35 ± 10.40) % at 50 μM. TPO photoinitiator showed the cell viability of (93.35 ± 8.08) % at 1 μM, (92.01 ± 10.21) % at 5 μM, (85.14 ± 11.94) % at 10 μM, (76.80 ± 9.36) % at 25 μM and (61.84 ± 15.60) % at 50 μM. TPO-L photoinitiator showed the cell viability of (95.91 ± 4.85) % at 1 μM, (95.48 ± 5.91) % at 5 μM, (95.57 ± 6.37) % at 10 μM, (91.85 ± 8.85) % at 25 μM and (80.48 ± 8.46) % at 50 μM. All photoinitiators showed no significant differences at concentrations of 1 ~ 10 μM. However, there revealed a significant difference in concentrations of 25 μM and 50 μM ($p < 0.05$).
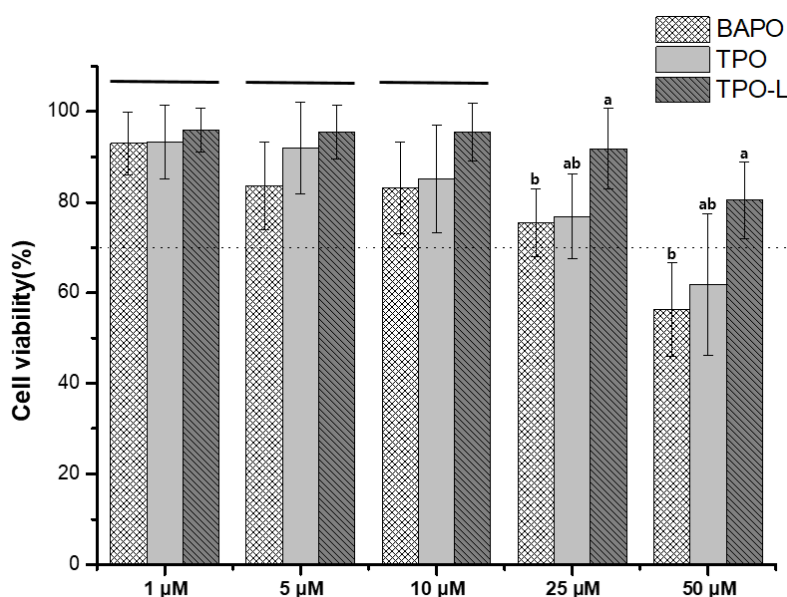
Figure 13. Cell viability of each photoinitiator. Each value represents the mean of 4 measurements, and the error bars represent the standard deviation of the mean (mean ± standard deviation). Differences in lowercase alphabetical letters above the bar graph indicate significant difference in each group at the same concentration ($p < 0.05$).

Horizontal bar: The cytotoxicity of each group was not significantly different from each other ($p > 0.05$).

3. Color stability

The color coordinates according to the conditions of the specimen are shown in Table 3. BAPO group showed lower values of a^* in the water sorption specimen and lower values of a^* and b^* in the irradiated and non-irradiated specimen compared to the baseline specimen. TPO and TPO-L groups showed similar values, with lower values of b^* in water sorption, irradiation and non-irradiated specimen compared to the baseline specimen.

The results of color change according to condition comparison of the testing groups are shown in Table 4. BAPO group revealed the highest ΔE values in all condition comparisons and showed a significant difference from other groups. The ΔE values of TPO and TPO-L groups showed no significant differences in all condition comparisons (p>0.05). TPO-L group showed the lowest ΔE value in all condition comparisons.

Table 3. Change of color coordinates.

Testing groups	Baseline			Water sorption			Irradiation			Non-irradiation		
	L^*	a^*	b^*	L^*	a^*	b^*	L^*	a^*	b^*	L^*	a^*	b^*
BAPO	36.2	1.21	7.79	39.63	-3.6	7.65	33.75	-0.53	1.52	36.9	-2.42	5.48
TPO	31.75	-0.23	1.82	32.01	-0.41	0.49	33.76	-0.39	0.74	33.76	-0.35	0.64
TPO-L	31.96	-0.28	1.40	32.31	-0.38	0.48	32.07	-0.34	0.52	31.47	-0.29	0.55

Table 4. Color change according to condition comparison (ΔE).

Testing groups	Baseline & water sorption	Baseline & irradiation	Baseline & non-irradiation	Irradiation & non-irradiation
BAPO	5.59 ± 1.43 [a]	7.21 ± 1.1 [a]	5.26 ± 1.15 [a]	5.65 ± 0.27 [a]
TPO	1.79 ± 0.35 [b]	2.73 ± 1.38 [b]	2.45 ± 1.34 [b]	2.59 ± 1.22 [b]
TPO-L	1.54 ± 0.61 [b]	1.24 ± 0.27 [b]	1.05 ± 1.43 [b]	0.75 ± 0.7 [b]

Same lowercase letter in the same column indicates no significant difference ($p > 0.05$).

4. Evaluation for dimensional accuracy

The 2D analysis by using color difference map was shown in Figure 14. The photoinitiator groups were shown in the color map compared to the original STL file. TPO and TPO-L groups revealed green line on the Z-axis and XY-axis. However, BAPO group revealed blue line on the Z-axis and yellow line on the XY-axis.

The results of 3D printing accuracy are shown in Table 5. Accuracy of the Z-axis revealed that the TPO-L group was closest to the true value. Z-axis value of TPO group was slightly out of tolerance levels but secondly similar to the true value. The accuracy of the XY-axis revealed that the TPO group was closest to the true value. XY-axis value of TPO-L group was within the tolerance levels and secondly similar to the true value. The BAPO group showed the lowest accuracy on the Z-axis and XY-axis. All groups showed a significant difference ($p<0.05$).

The accuracy of base plane was not significantly different in all groups ($p>0.05$).
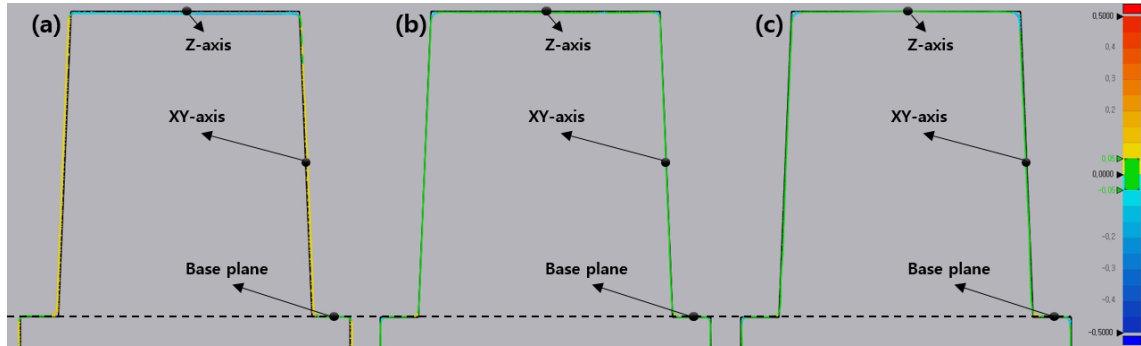
Figure 14. 2D analysis of accuracy by using color difference map (Green represents good fit, yellow or red represents positive error, and blue represents negative error). (a) 2D analysis of BAPO group, (b) 2D analysis of TPO group, (c) 2D analysis of TPO-L group. The black dashed line shows the base plane. Each value represents the mean of 3 measurements.

Table 5. Mean and standard deviation of 3D printing accuracy according to three photoinitiators.

Testing groups	Z-axis (mm)	XY-axis (mm)	Base plane (mm)
BAPO	- 0.102 ± 0.037 [c]	0.06 ± 0.030 [c]	0.013 ± 0.018 [a]
TPO	- 0.053 ± 0.003 [b]	- 0.021 ± 0.013 [a]	0.018 ± 0.017 [a]
TPO-L	- 0.007 ± 0.005 [a]	- 0.048 ± 0.021 [b]	0.028 ± 0.018 [a]

Same lowercase letter in the same column indicates no significant difference (p>0.05).

5. Degree of conversion

The results of the degree of conversion are shown in Table 6. All groups showed a degree of conversion of more than 80 %. The degree of conversion increased gradually in order of TPO, BAPO, and TPO-L, but there was no significant difference (p>0.05).

Table 6. Degree of conversion of each group.

Testing groups	Degree of conversion (%)
BAPO	83.16 ± 3.07 [a]
TPO	81.75 ± 3.14 [a]
TPO-L	85.57 ± 3.87 [a]

Same lowercase letter in the same column indicates no significant difference (p>0.05).

6. Mechanical properties

6.1. Flexural strength

The results of the three-point flexural strength test are shown in Figure 15. The BAPO group had a strength of (26.18 ± 0.96) MPa, which was a statistically not significant difference from (25.75 ± 1.09) MPa for TPO group and (25.23 ± 1.36) MPa for TPO-L group ($p>0.05$).
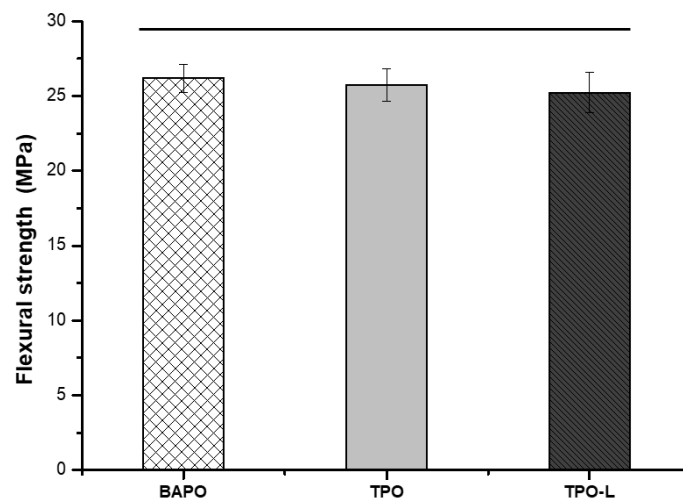
Figure 15. Flexural strength of each group. Each value represents the mean of 15 measurements, and the error bars represent the standard deviation of the mean (mean ± standard deviation). Horizontal bar: The strength of each group was not significantly different from each other ($p>0.05$).

6.2. Microhardness

The results of the Knoop hardness are shown in Figure 16. The hardness values of each group were BAPO group (141.43 ± 10.38), TPO group (141.67 ± 14.94), and TPO-L group (131.1 ± 9.73). The results showed no significant differences for each group in the hardness ($p > 0.05$).
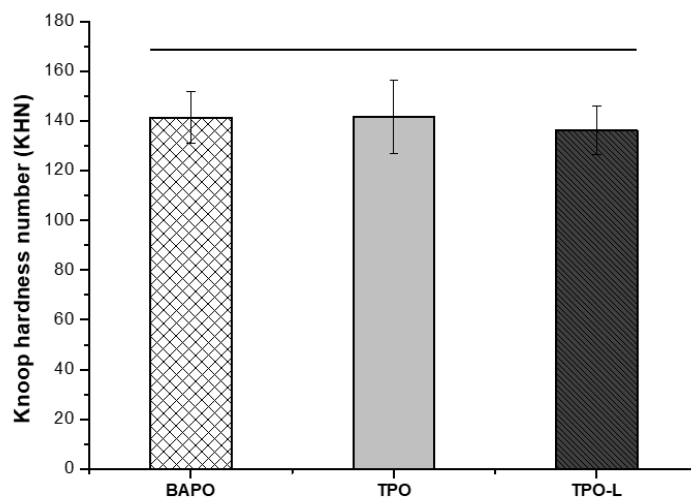
Figure 16. Microhardness of each group. Each value represents the mean of 10 measurements, and the error bars represent the standard deviation of the mean (mean ± standard deviation) Horizontal bar: The microhardness of each group was not significantly different from each other ($p > 0.05$).

7. Physical properties

7.1. Water sorption and solubility

The results of water sorption and solubility are shown in Table 7. The water sorption results were the lowest value in BAPO group and the highest value in TPO-L group, and showed a significant difference ($p<0.05$).

The results of water solubility were no significant difference in TPO and TPO-L groups. However, BAPO group showed significantly lower values compared to other groups ($p<0.05$).

Table 7. Water sorption and solubility of each group.

Testing groups	Water sorption ($\mu g/mm^3$)	Solubility ($\mu g/mm^3$)
BAPO	62.50 ± 1.25 [a]	8.42 ± 0.54 [a]
TPO	64.31 ± 0.65 [ab]	10.44 ± 0.42 [b]
TPO-L	65.80 ± 2.84 [b]	10.54 ± 0.42 [b]

Same lowercase letter in the same column indicates no significant difference ($p>0.05$).

IV. DISCUSSION

Photoinitiators play a key role in the photopolymerization process (Dumur, 2020). The photoinitiation system not only determines the mechanism of the reaction but also affects the final properties of the polymer, such as the degree of conversion and mechanical properties. In addition, physical properties, cytotoxicity and accuracy are very important as the dental 3D printed resin is placed in the patient's oral cavity (Aati et al., 2021). The selection of an appropriate photoinitiator is essential to obtain the properties of the desired polymer. A suitable photoinitiator must be compatible between the absorption characteristics of photoinitiators and the emission characteristics of the light source, to be non-cytotoxic and prevent the cured resin from yellowing (Tomal and Ortyl, 2020).

The residual monomers and additives are free to diffuse out from the cured materials. They may be released into surrounding tissues and may have potential toxic effects. The photoinitiator was identified as one of the main released components in extracts of resin-based materials (Chang et al., 2015). Cytotoxicity of 3D printed resin groups was tested based on ISO 10993-5:2009 (ISO, 2009). All groups showed significant differences. The group with the lowest cell viability was the BAPO group. According to the references, the BAPO shows 50 ~ 250 fold higher cytotoxicity than CQ and induces more than 50% cytotoxicity in human oral keratinocytes cells at concentrations greater than 10 μM. (Popal et al., 2018). In addition, the BAPO was indicated that exhibits a more obvious cytotoxicity response to the HEK293, LO2 and HUVEC cell types (Zeng et al., 2021). The residual monomers and additives could affect cell viability. Because the degree of conversion results of three photoinitiator group were similar, the amount of residual monomer could be expected to be similar in each photoinitiator group. To evaluate the toxicity of the photoinitiator as an additive, the cytotoxicity of the photoinitiator was measured. The cytotoxicity results of each photoinitiator were shown in Figure 13. All photoinitiators showed no significant differences at concentrations of 1 ~ 10 μM. However, there revealed a significant difference in concentrations of 25 μM and 50 μM. In particular, BAPO and TPO photoinitiators were high cytotoxic at a concentration of 50 μM. TPO-L photoinitiator showed the highest cell viability at all concentrations. BAPO and TPO photoinitiators increased cytotoxicity in L929 cells in a concentration-dependent. According to the references, the TPO reduced cell viability in a dose-dependent manner, and TPO was much more cytotoxic than CQ in human pulp-derived cells (Almeida et al., 2020). Thus, a high concentration of BAPO and TPO is not recommended for clinical application. The TPO-L group exhibits significantly lower cytotoxicity than other groups. In other studies, TPO-L was the least toxic of the seven photoinitiators at concentrations of 1 ~ 50 μM (Zeng et al., 2021). Therefore, TPO-L is more promising to be broadly applied to clinical

practice.

Color stability is an important factor in the success and longevity of restorations (Stawarczyk et al., 2012). The hydrophilicity or hydrophobicity of the restorative material, the amount of photoinitiator or inhibitor, the degree of polymerization and the composition of resin matrix have a strong effect on discoloration (Van Landuyt et al., 2007). The CIE $L^*a^*b^*$ color order system is commonly used in dental research. In this system, the location of a particular shade in the color space is defined by three coordinates: L^*, a^*, and b^*. L^* describes the lightness of the object being evaluated. The a^* value defines the color on the red-green axis and b* on the yellow-blue axis. The measure of the total color difference between two objects is described by ΔE (Heydecke et al., 2001). In Table 3, the BAPO group shown that the value of a^* decreases at the water absorption condition and the value of b^* decreases at the irradiation condition compared to the baseline condition. Therefore, it was revealed that the discoloration of BAPO group was considerably affected by immersion and light. Also, TPO and TPO-L groups found that b^* values decreased and became transparent at water absorption, irradiation and non-irradiation conditions. Table 4 shown ΔE values. ΔE is important in quantifying the color difference between two specimens. Under clinical conditions, ΔE has to approach 3.3 or higher before the human eye can detect a color difference (Rodríguez et al., 2019). The TPO-L and TPO groups had a ΔE value of less than 3.3 in all condition comparisons. The TPO-L group represented the lowest ΔE value in all condition comparisons and showed excellent color stability. The TPO group had secondly good color stability and no significant difference from the ΔE value of the TPO-L group (p>0.05). The BAPO group had a ΔE value of higher than 3.3 for all condition comparisons. The cause of the significant color difference in the BAPO group is the discoloration of the baseline specimen. It can be considered that the cause of the discoloration is that the acyl radicals remaining after polymerization are generated as colored radicals (Albuquerque et al., 2013). The photoinitiators used in the experiment generate an acyl radical and a phosphonyl radical after absorption of light energy. But, In the BAPO molecule structure, two carbonyl groups interact with the central phosphonyl group, leading to four reactive radicals (Meereis et al., 2014; Salgado et al., 2017). As a result, radicals that were not involved in the polymerization became present, and the residual radicals were form colored radicals, which was considered the specimen was changed color. Also, water sorption specimen was found that the components of the immersed specimen were eluted and there were no residual radicals, the color of specimens changed into the color of the original mixed 3D printing resin.

Low accuracy can lead to problems such as the need for chairside adjustment or compromised longevity of the restoration (Park et al., 2020). The accuracy of the printed objects is correlated

to the front polymerization kinetics of formulated resins (Vitale and Cabral, 2016). The BAPO group showed significantly higher negative errors from the Z-axis than the other groups ($p<0.05$). The formation of a polymer network with a denser structure results in volumetric contraction or shrinkage (Acosta Ortiz et al., 2015). Many factors affect the shrinkage in dental resin. These can be separated into material formulation factors and material polymerization factors (Ferracane, 2005). Photoinitiators affected shrinkage as material formulation factors. BAPO photoinitiator revealed greater shrinkage than other photoinitiators. Also, the BAPO group showed significantly higher positive errors from the XY-axis than the other groups ($p<0.05$). These reasons are due to the pixel size of the 3D printer and the high absorbance of the BAPO photoinitiator. The pixel size of the used 3D printer in the experiment was 62.5 μm. When printing the specimen, the BAPO group was over-curing by one-pixel size than the designed value. It can be expected that this resulted in the error of the XY-axis in the BAPO group. On the other hand, TPO and TPO-L photoinitiators have less absorbance than BAPO photoinitiator. Therefore, over-curing does not occur on the XY-axis.

Degree of conversion is the most important factor in resin materials. This is because it can affect mechanical and physical properties and cytotoxicity (Eshmawi et al., 2018; Fujioka-Kobayashi et al., 2019; Lin et al., 2020). TPO and TPO-L can undergo α-cleavage in the excited triplet state of the C-P bonds after absorption of light energy, generating two free radicals per molecule. On the other hand, BAPO forms four radicals per molecule (Neumann et al., 2006). However, the degree of conversion was not significantly different in all groups ($p>0.05$).

3D printed resin needs to have appropriate mechanical properties because the 3D printed restoration can encounter mechanical stresses when placed on areas that are subjected to force of mastication (Dejak et al., 2003). The mechanical properties of the resin depend on the resin matrix, degree of conversion and the presence of filler (Gonçalves et al., 2009; Rodríguez et al., 2019). In this study, all groups had the same resin matrix mixture. Figure 15 showed that the average flexural strength in all groups was 25 ~ 26 MPa. Figure 16 showed that the average Knoop hardness number in all groups was 131 ~ 141 KHN. All groups were able to confirm that the mechanical properties were similar without significant differences. In Table 6, all groups showed no significant difference in the degree of conversion. This suggests that the photoinitiators used in the experiment have a similar polymerization effect. The ISO 4049:2019 (ISO, 2019) standard requires a minimum 50 MPa of flexural strength. The reason for the low result values from all groups was that no filler has been added. The fillers can improve mechanical properties depending on the type and loading ratio (Randolph et al., 2016; Rodríguez et al., 2019). In this research, in order to remove the variables, an 3D printing resin was used in which the resin substrate and

photoinitiator were mixed without inorganic fillers.

Water sorption occurs mainly at the resin matrix. The water absorbed by the resin matrix could cause hydrolytic degradation and may affect the resin materials (El-Hadary and Drummond, 2000). When the resin specimens are immersed in water, the unreacted monomer may dissolve and are leached out of the specimens (Tuna et al., 2008). These results in loss of weight and can be measured as solubility. Therefore, the water sorption and solubility may affect the initial dimensional change of resin, the clinical performance, and the biocompatibility (Toledano et al., 2003). Even though the ISO 4049 standard is not the proper standard for our tested material, its main composition is similar to polymer-based restorative materials of ISO 4049. The ISO 4049:2019 (ISO, 2019) standard requires the following maximum values: water sorption ≤ 40 $\mu g/mm^3$ and solubility ≤ 7.5 $\mu g/mm^3$. All groups had higher water absorption and solubility values than the ISO 4049 standard. These causes are due to the absence of filler in the tested material. Filler-added resin materials showed much lower water absorption and solubility values than only resin matrix materials (Ferracane, 2006; Sokolowski et al., 2018).

Current studies have measured that the result values of mechanical and physical properties are lower than the ISO standard. Further studies are needed with the addition of additives such as fillers to improve mechanical and physical properties.

V. CONCLUSION

An ideal photoinitiator of 3D printing resin should be had biocompatibility, color stability, high degree of conversion and 3D printing accuracy. But the BAPO and TPO photoinitiators, which are mainly used for 3D printing, have disadvantages such as cytotoxicity and discoloration. The purpose of this study is to investigate whether the TPO-L photoinitiator could be replaced BAPO and TPO photoinitiators. Within the laboratory conditions of this study, the following results and conclusions were drawn:

1. In the cell viability of the 3D-printed resin groups, TPO-L group had the highest cell viability and the BAPO group had the lowest cell viability. Also, the cell viability of the photoinitiator according to the concentration, TPO-L photoinitiator had the highest cell viability at all concentrations, and BAPO photoinitiator had the lowest cell viability at 25 μM and 50 μM ($p<0.05$). Therefore, the null hypothesis that no significant difference in cytotoxicity according to the photoinitiator was rejected.

2. As a result of the color stability test, the TPO-L group showed the lowest ΔE values and was not significantly different from the TPO group. However, the BAPO group showed high discoloration in the color difference of all conditions comparison and there was a significant difference from the other groups ($p<0.05$). Therefore, the null hypothesis that no significant difference in color stability according to the photoinitiator was rejected.

3. Z-axis accuracy of the TPO-L group was the closest to the true value. XY-axis accuracy of the TPO group was very close to the true value. In the BAPO group, the result values of the Z-axis and XY-axis accuracy were the farthest from the true values. The accuracy of the Z-axis and XY-axis showed significant differences among the groups. All photoinitiator groups had no significant difference in the values of base plan accuracy ($p<0.05$). Therefore, the null hypothesis that no significant difference in 3D printing accuracy according to the photoinitiator was rejected.

4. Degree of conversion was no significant difference in all groups ($p>0.05$). Therefore, the null hypothesis that no significant difference in the degree of conversion according to the photoinitiator was accepted.

5. In mechanical properties, the deviations of the result values for all groups were small. All groups showed no significant differences in flexural strength and microhardness ($p>0.05$).

Therefore, the null hypothesis that no significant difference in mechanical properties according to the photoinitiator was accepted.

6. In water sorption and solubility, the BAPO group showed less value than the other groups ($p < 0.05$). Therefore, the null hypothesis that no significant difference in physical properties according to the photoinitiator was rejected.

In this study, experimental results have shown that photoinitiators can significantly affect the dental 3D printed resin. The TPO-L group was similar or showed better experimental results than the BAPO and TPO groups.

In particular, TPO-L photoinitiator showed excellent biocompatibility and color stability and showed sufficient accuracy for use in 3D printing.

Therefore, the TPO-L photoinitiator can solve the problems of BAPO and TPO photoinitiators and can be sufficiently used as a photoinitiator for dental 3D printing resin.

VI. REFERENCES

Aati S, Akram Z, Ngo H, Fawzy AS (2021). Development of 3D printed resin reinforced with modified ZrO2 nanoparticles for long-term provisional dental restorations. *Dental Materials*.

Abduo J, Lyons K, Bennamoun M (2014). Trends in computer-aided manufacturing in prosthodontics: a review of the available streams. *International journal of dentistry* 2014.

Acosta Ortiz R, Savage Gomez AG, Berlanga Duarte ML, Garcia Valdez AE (2015). The effect of a dithiol spiroorthocarbonate on mechanical properties and shrinkage of a dental resin. *Designed Monomers and Polymers* 18(1): 73-78.

Albuquerque PPA, Moreira AD, Moraes RR, Cavalcante LM, Schneider LFJ (2013). Color stability, conversion, water sorption and solubility of dental composites formulated with different photoinitiator systems. *Journal of dentistry* 41: e67-e72.

Almeida SM, Meereis CT, Leal FB, Carvalho RV, Boeira PO, Chisini LA, et al. (2020). Evaluation of alternative photoinitiator systems in two-step self-etch adhesive systems. *Dental Materials* 36(2): e29-e37.

Andrzejewska E (2001). Photopolymerization kinetics of multifunctional monomers. *Progress in polymer science* 26(4): 605-665.

Chang M-C, Lin L-D, Wu M-T, Chan C-P, Chang H-H, Lee M-S, et al. (2015). Effects of camphorquinone on cytotoxicity, cell cycle regulation and prostaglandin E2 production of dental pulp cells: role of ROS, ATM/Chk2, MEK/ERK and hemeoxygenase-1. *PLoS One* 10(12): e0143663.

de Oliveira DCRS, Rocha MG, Correa IC, Correr AB, Ferracane JL, Sinhoreti MAC (2016). The effect of combining photoinitiator systems on the color and curing profile of resin-based composites. *Dental Materials* 32(10): 1209-1217.

Dejak B, Młotkowski A, Romanowicz M (2003). Finite element analysis of stresses in molars during clenching and mastication. *The Journal of prosthetic dentistry* 90(6): 591-597.

Della Bona A, Cantelli V, Britto VT, Collares KF, Stansbury JW (2021). 3D printing restorative materials using a stereolithographic technique: a systematic review. *Dental Materials*.

Dumur F (2020). Recent advances on carbazole-based photoinitiators of polymerization. *European Polymer Journal* 125: 109503.

El-Hadary A, Drummond JL (2000). Comparative study of water sorption, solubility, and tensile bond strength of two soft lining materials. *The Journal of prosthetic dentistry* 83(3): 356-361.

Eshmawi YT, Al-Zain AO, Eckert GJ, Platt JA (2018). Variation in composite degree of conversion and microflexural strength for different curing lights and surface locations. *The Journal of the American Dental Association* 149(10): 893-902.

Ferracane JL (2005). Developing a more complete understanding of stresses produced in dental composites during polymerization. *Dental Materials* 21(1): 36-42.

Ferracane JL (2006). Hygroscopic and hydrolytic effects in dental polymer networks. *Dental Materials* 22(3): 211-222.

Fujioka-Kobayashi M, Miron RJ, Lussi A, Gruber R, Ilie N, Price RB, et al. (2019). Effect of the degree of conversion of resin-based composites on cytotoxicity, cell attachment, and gene expression. *Dental materials* 35(8): 1173-1193.

Gonçalves F, Kawano Y, Pfeifer C, Stansbury JW, Braga RR (2009). Influence of BisGMA, TEGDMA, and BisEMA contents on viscosity, conversion, and flexural strength of experimental resins and composites. *European journal of oral sciences* 117(4): 442-446.

Heydecke G, Zhang F, Razzoog ME (2001). In vitro color stability of double-layer veneers after accelerated aging. *The Journal of prosthetic dentistry* 85(6): 551-557.

Ikemura K, Endo T (2010). A review of the development of radical photopolymerization initiators used for designing light-curing dental adhesives and resin composites. *Dental Materials Journal*: 1009140075-1009140075.

ISO (2009). 10993–5: 2009 Biological evaluation of medical devices—part 5: tests for in vitro cytotoxicity. *International Organization for Standardization, Geneva.*

ISO (2012). Biological evaluation of medical devices—part 12: Sample preparation and reference materials (ISO 10993–12: 2012).

ISO (2019). Dentistry-Polymer-based Restorative Materials. ISO.

Lai H, Zhu D, Xiao P (2019). Yellow triazine as an efficient photoinitiator for polymerization and 3D printing under LEDs. *Macromolecular Chemistry and Physics* 220(18): 1900315.

Lin C-H, Lin Y-M, Lai Y-L, Lee S-Y (2020). Mechanical properties, accuracy, and cytotoxicity of UV-polymerized 3D printing resins composed of Bis-EMA, UDMA, and TEGDMA. *The Journal of prosthetic dentistry* 123(2): 349-354.

Manojlovic D, Dramićanin MD, Lezaja M, Pongprueksa P, Van Meerbeek B, Miletic V (2016). Effect of resin and photoinitiator on color, translucency and color stability of conventional and low-shrinkage model composites. *Dental materials* 32(2): 183-191.

Meereis CT, Leal FB, Lima GS, de Carvalho RV, Piva E, Ogliari FA (2014). BAPO as an alternative photoinitiator for the radical polymerization of dental resins. *Dental materials* 30(9): 945-953.

Moon W, Kim S, Lim B-S, Park Y-S, Kim RJ-Y, Chung SH (2021). Dimensional Accuracy Evaluation of Temporary Dental Restorations with Different 3D Printing Systems. *Materials* 14(6): 1487.

Neumann MG, Schmitt CC, Ferreira GC, Corrêa IC (2006). The initiating radical yields and the efficiency of polymerization for various dental photoinitiators excited by different light curing units. *Dental Materials* 22(6): 576-584.

Park J-M, Jeon J, Koak J-Y, Kim S-K, Heo S-J (2020). Dimensional accuracy and surface characteristics of 3D-printed dental casts. *The Journal of prosthetic dentistry.*

Park M-E, Shin S-Y (2018). Three-dimensional comparative study on the accuracy and reproducibility of dental casts fabricated by 3D printers. *The Journal of prosthetic dentistry* 119(5): 861. e861-861. e867.

Peutzfeldt A (1997). Resin composites in dentistry: the monomer systems. *European journal of oral sciences* 105(2): 97-116.

Pongprueksa P, Miletic V, Janssens H, Van Landuyt KL, De Munck J, Godderis L, et al. (2014). Degree of conversion and monomer elution of CQ/amine and TPO adhesives. *Dental Materials* 30(6): 695-701.

Popal M, Volk J, Leyhausen G, Geurtsen W (2018). Cytotoxic and genotoxic potential of the type I photoinitiators BAPO and TPO on human oral keratinocytes and V79 fibroblasts. *Dental Materials* 34(12): 1783-1796.

Randolph LD, Palin WM, Leloup G, Leprince JG (2016). Filler characteristics of modern dental resin

composites and their influence on physico-mechanical properties. *Dental Materials* 32(12): 1586-1599.

Revilla-León M, Özcan M (2019). Additive manufacturing technologies used for processing polymers: current status and potential application in prosthetic dentistry. *Journal of Prosthodontics* 28(2): 146-158.

Rodríguez HA, Kriven WM, Casanova H (2019). Development of mechanical properties in dental resin composite: Effect of filler size and filler aggregation state. *Materials Science and Engineering: C* 101: 274-282.

Salgado VE, Cavassoni D, Gonçalves APR, Pfeifer C, Moraes RR, Schneider LF (2017). Photoinitiator system and water effects on C=C conversion and solubility of experimental etch-and-rinse dental adhesives. *International Journal of Adhesion and Adhesives* 72: 6-9.

Schneider LFJ, Cavalcante LM, Prahl SA, Pfeifer CS, Ferracane JL (2012). Curing efficiency of dental resin composites formulated with camphorquinone or trimethylbenzoyl-diphenyl-phosphine oxide. *Dental materials* 28(4): 392-397.

Sokolowski K, Szczesio-Wlodarczyk A, Bociong K, Krasowski M, Fronczek-Wojciechowska M, Domarecka M, et al. (2018). Contraction and Hydroscopic Expansion Stress of Dental Ion-Releasing Polymeric Materials. *Polymers* 10(10): 1093.

Stansbury JW (2012). Dimethacrylate network formation and polymer property evolution as determined by the selection of monomers and curing conditions. *Dental Materials* 28(1): 13-22.

Stansbury JW, Idacavage MJ (2016). 3D printing with polymers: Challenges among expanding options and opportunities. *Dental materials* 32(1): 54-64.

Stawarczyk B, Sener B, Trottmann A, Roos M, Oezcan M, Hämmerle CH (2012). Discoloration of manually fabricated resins and industrially fabricated CAD/CAM blocks versus glass-ceramic: effect of storage media, duration, and subsequent polishing. *Dental materials journal* 31(3): 377-383.

Steyrer B, Neubauer P, Liska R, Stampfl J (2017). Visible light photoinitiator for 3D-printing of tough methacrylate resins. *Materials* 10(12): 1445.

Toledano M, Osorio R, Osorio E, Fuentes V, Prati C, Garcıa-Godoy F (2003). Sorption and solubility of resin-based restorative dental materials. *Journal of dentistry* 31(1): 43-50.

Tomal W, Ortyl J (2020). Water-soluble photoinitiators in biomedical applications. *Polymers* 12(5): 1073.

Tuna SH, Keyf F, Gumus HO, Uzun C (2008). The evaluation of water sorption/solubility on various acrylic resins. *European journal of dentistry* 2: 191.

Van Landuyt K, Nawrot T, Geebelen B, De Munck J, Snauwaert J, Yoshihara K, et al. (2011). How much do resin-based dental materials release? A meta-analytical approach. *Dental Materials* 27(8): 723-747.

Van Landuyt KL, Snauwaert J, De Munck J, Peumans M, Yoshida Y, Poitevin A, et al. (2007). Systematic review of the chemical composition of contemporary dental adhesives. *Biomaterials* 28(26): 3757-3785.

Van Noort R (2012). The future of dental devices is digital. *Dental materials* 28(1): 3-12.

Vitale A, Cabral JT (2016). Frontal conversion and uniformity in 3D printing by photopolymerisation. *Materials* 9(9): 760.

Zeng B, Cai Z, Lalevée J, Yang Q, Lai H, Xiao P, et al. (2021). Cytotoxic and cytocompatible comparison among seven photoinitiators-triggered polymers in different tissue cells. *Toxicology in Vitro* 72: 105103.

ABSTRACT (IN KOREAN)

TPO-L 광개시제를 함유한 3D 프린팅 레진의 생체 적합성 및 색상 안정성

<지도교수 권 재 성 >

연세대학교 대학원 응용생명과학과

김 기 태

목적

3D 프린팅 시스템은 제작 과정의 간소화와 제작 시간 단축으로 치과분야에 많은 영향을 미치고 있다. DLP 방식의 3D 프린팅에 사용하는 재료는 광중합 레진이다. BAPO와 TPO 광개시제는 높은 중합효율, 우수한 중합속도의 장점으로 인해 3D 프린팅 레진의 광개시제로 사용되고 있다. 그러나 세포 독성과 변색으로 인한 단점으로 한계가 있었다. 반면, TPO-L은 생체적합성이 좋고 색 안정성이 뛰어난 장점을 갖고 있으나 아직까지 DLP 방식의 3D 프린팅 레진의 광개시제로 사용한 연구는 드물었다. 따라서 본 연구의 목적은 TPO-L을 광개시제로 사용하여 3D 프린팅 레진에 대한 세포독성, 색 안정성, 치수 정확도, 중합율, 기계적 및 물리적 특성을 시험하고 광개시제로서의 활용가능성을 평가함에 있다.

재료 및 방법

연구를 수행하기 위해 동일한 레진 기질 (70% UDMA, 20% Bis-EMA, 10% TEGDMA)을 사용하였다. 광개시제로는 BAPO, TPO, TPO-L을 사용하였고 3D 프린팅 레진 용액을 만들기 위해 레진 기질에 0.1 mol%로 혼합되었다. 시편은 CAD 프로그램을 사용하여 디자인하였고 DLP 방식의 3D 프린터에서 출력하였다. 출력된 시편은 IPA로 5분간 세척을 진행하고 후경화기에서 15분간 중합되었다. 실

험은 세포 독성, 색 안정성, 치수 정확도, 중합율, 기계적 및 물리적 특성을 측정하였다.

결과

3D 프린팅된 레진 그룹의 세포독성 실험에서 TPO-L 그룹은 BAPO와 TPO 그룹보다 유의하게 높은 세포 생존율을 보였다 ($p < 0.05$). 농도에 따른 광개시제의 세포독성 실험에서 TPO-L 광개시제가 모든 농도에서 높은 세포 생존율을 보였고 BAPO와 TPO는 $25 \mu M$ 과 $50 \mu M$ 농도에서 유의하게 낮은 세포 생존율을 보였다 ($p < 0.05$). 색 안정성 실험에서 TPO-L 그룹은 가장 높은 색 안정성을 보였으며 TPO 그룹과 유의한 차이를 보이지 않았다 ($p > 0.05$). 그러나 BAPO 그룹은 가장 낮은 색 안정성을 보여주었고 다른 그룹들과 유의한 차이를 보였다 ($p < 0.05$). 치수 정확도 실험은 Z축에서 TPO-L 그룹, TPO 그룹, BAPO 그룹 순으로 참 값과 가까웠다. XY축에서는 TPO 그룹, TPO-L 그룹, BAPO 그룹 순으로 참 값과 가까웠다. 치수 정확도의 모든 그룹은 유의한 차이가 있었다 ($p < 0.05$). 중합율과 기계적 특성은 모든 그룹이 유의한 차이가 없었다 ($p > 0.05$). 물리적 특성인 물 흡수도 및 용해도는 BAPO그룹이 유의하게 낮은 결과값을 보였다 ($p < 0.05$).

중요성

본 연구를 통해 TPO-L 광개시제는 우수한 생체 적합성과 높은 색 안정성을 보였으며 3D 프린팅 레진에 사용하기에 적합한 치수 정확도를 나타내었다. 따라서 TPO-L 광개시제는 BAPO 및 TPO 광개시제의 단점을 해결할 수 있으며 3D 프린팅 레진의 광개시제로 충분히 활용이 가능하다.

핵심되는 말: 3D 프린팅 정확도, 색 안정성, 세포독성, DLP 3D 프린팅, TPO-L 광개시제